YALE
PEABODY
MUSEUM

P.O. BOX 208118 | NEW HAVEN CT 06520-8118 USA | PEABODY.YALE. EDU

JOURNAL OF MARINE RESEARCH

The *Journal of Marine Research,* one of the oldest journals in American marine science, published important peer-reviewed original research on a broad array of topics in physical, biological, and chemical oceanography vital to the academic oceanographic community in the long and rich tradition of the Sears Foundation for Marine Research at Yale University.

An archive of all issues from 1937 to 2021 (Volume 1–79) are available through EliScholar, a digital platform for scholarly publishing provided by Yale University Library at https://elischolar.library.yale.edu/.

Requests for permission to clear rights for use of this content should be directed to the authors, their estates, or other representatives. The *Journal of Marine Research* has no contact information beyond the affiliations listed in the published articles. We ask that you provide attribution to the *Journal of Marine Research*.

Yale University provides access to these materials for educational and research purposes only. Copyright or other proprietary rights to content contained in this document may be held by individuals or entities other than, or in addition to, Yale University. You are solely responsible for determining the ownership of the copyright, and for obtaining permission for your intended use. Yale University makes no warranty that your distribution, reproduction, or other use of these materials will not infringe the rights of third parties.

This work is licensed under a Creative Commons Attribution-NonCommercial-ShareAlike 4.0 International License.
https://creativecommons.org/licenses/by-nc-sa/4.0/

Journal of Marine Research, 62, 37–65, 2004

Representativeness of meridional hydrographic sections in the western South Atlantic

by A. M. Thurnherr[1] and K. G. Speer[2]

ABSTRACT

Many studies of the oceanic circulation are based on data collected during quasi-synoptic hydrographic surveys. After spatial averaging, to filter out the effects of mesoscale variability, it is often explicitly or implicitly assumed that the synoptic hydrographic gradients are representative of a quasi-steady "mean" state. Climatological tracer fields and float data at the depth of the North Atlantic Deep Water in the western South Atlantic (Brazil Basin) support the notion of a quasi-steady mean circulation characterized by alternating bands of primarily zonal flow with meridional scales of several hundreds of km. Visually, the mean circulation appears to dominate three samples of the large-scale meridional-density-gradient field taken between 1983 and 1994. A quantitative comparison reveals, however, that the baroclinic temporal variability of the zonal velocities is of the same magnitude as the mean and is associated with similar spatial scales. The synoptic geostrophic flow field is, therefore, only marginally representative of the mean state. Thus, the data do not support one of the central assumptions of reference-velocity methods, such as linear box-inverse models and the β-spiral, because baroclinic temporal variability renders the equation systems underlying these methods inconsistent. A modal decomposition of the temporally varying baroclinic zonal velocity field in the Brazil Basin indicates that the first two dynamical modes dominate, accounting for ≈90% of the rms velocities. The residual flow field that remains after removing the first two baroclinic modes from the three synoptic samples is dominated by the mean circulation. However, its magnitude is not sufficient to account for the float and tracer observations. Therefore, it is necessary to determine the projection of the mean zonal velocities onto the barotropic and the first two baroclinic modes in order to diagnose fully the mean zonal circulation in the western South Atlantic. There is evidence that the representativeness of synoptic hydrographic sections in other regions may be similarly marginal.

1. Introduction

Determining the quasi-steady or mean circulation over periods of a decade or more is one of the main goals of large-scale physical oceanography. One of the most widely used methods is to determine the vertical shear of the geostrophic velocity field from hydrographic measurements, usually collected as (quasi-)synoptic data sets on time scales of weeks. Using such samples to draw inferences about a mean state requires an assumption

1. Lamont Doherty Earth Observatory, Columbia University, P. O. Box 1000, Palisades, New York, 10964-1000, U.S.A. ***email: ant@ldeo.columbia.edu***

2. Department of Oceanography, Florida State University, Tallahassee, Florida, 32306, U.S.A.

of representativeness on the time and space scales of interest. In the presence of temporal variability a single synoptic sample cannot be expected to be truly representative. Formal methods, such as linear inversions, therefore require estimates of the temporal variability of the sampled fields, which are often assumed to be normally distributed about a mean state. The standard deviations are commonly assigned more-or-less arbitrarily, although output from numerical models is sometimes used (e.g. Ganachaud, 1999). In the context of this study we will call a single sample representative if it is significantly different from zero. (In practice, representativeness will be determined from multiple samples by comparing the magnitude of the sample mean to the standard deviation: if the magnitude of the mean is larger than the standard deviation, a single sample is expected to be representative; if the magnitudes are similar, the expected representativeness will be called marginal.) Applying this definition to hydrographic data implies that there is no information about the mean circulation to be gained by calculating geostrophic shear in regions where the synoptic density gradients are not representative—an assumption of zero shear is equally reasonable.

Direct velocity measurements indicate that, on small spatial scales, the instantaneous oceanic flow field is generally dominated by temporal variability. Therefore, temporal averaging is required in order to extract the signal associated with the mean circulation. Very few (if any) hydrographic sections have been occupied often enough to construct representative temporal averages on small spatial scales. Ignoring the high-frequency ageostrophic motions associated with the tides and with the internal-wave field, the dominant temporal variability is found in what is commonly called the mesoscale, the spatial scales of which range roughly from the first baroclinic deformation radius (typically 10–30 km; e.g. Gill, 1982) to several hundred km (e.g. Wunsch, 1981; Armi and Stommel, 1983). In practice it is, therefore, often assumed that spatial averaging over scales exceeding the mesoscale renders hydrographic snapshots representative of the mean. Linear box-inverse models (e.g. Wunsch, 1996) are a case in point: steady-state mass- and tracer-conservation constraints, applied to closed boxes between hydrographic sections, imply that the fluxes integrated along each edge are considered representative over the spatial scales of the boxes and the temporal scales associated with the sampling. The spatial scales of interest range from entire ocean basins to a few hundred km (e.g. Vanicek and Siedler, 2002). Typical temporal scales of observations are several years to decades, e.g. in the case of the World Ocean Circulation Experiment (WOCE) hydrographic data set. The fundamental purpose of standard box-inverse models (and other linear inverse methods, such as the β-spiral) is to determine the integration constants that are required to produce velocity profiles from vertical geostrophic shear. Any baroclinic temporal variability on the spatial scales of interest renders the underlying linear equation systems inconsistent, increasing their residuals.

The available evidence for representativeness of synoptic hydrographic sections is ambiguous. Wunsch (1981) qualitatively compares an upper ocean (above 2500 m) potential-temperature repeat section between northern North America and the Caribbean

and notes that the temperature fields were similar in 1873 and in 1954/58. From this he infers that the large-scale baroclinic structure of the circulation in that particular region has remained stable for many decades. Given the sampling resolution (and, presumably, the accuracy) of the 19th-century section, the similarities are essentially restricted to regions near the western boundary and above 1000 m, i.e. where the flow is strong. In the remainder of the temperature sections the horizontal gradients are small and the similarities between the two samples cannot be assessed visually. More quantitatively, Armi and Stommel (1983) analyze four triangular hydrographic surveys of a portion of the subtropical gyre in the North Atlantic. Above 1000 m they find variability of the large-scale (order 1000 km) geostrophic shear as large as the shear itself, i.e. the snapshots are only marginally representative. Below 1000 m the four baroclinic-shear samples are dissimilar. When entire trans-oceanic sections between continents are integrated the temporal variability related to horizontally shifting currents disappears. In their analysis of two transatlantic repeat sections, Roemmich and Wunsch (1985) find that quasi-synoptic basin-wide averages of the geostrophic velocities are qualitatively similar, but that the transport differences between repeat observations in 18 layers are of the same order as the transports themselves; i.e., the individual samples are again only marginally representative. In spite of this evidence suggesting that synoptic snapshots of the baroclinic shear cannot generally be considered representative of the mean, except perhaps in regions of strong currents, representativeness is usually assumed in large-scale circulation studies based on hydrographic data. Notable exceptions are ocean-state estimates that adjust the hydrographic fields in addition to determining reference velocities (see discussion in Talley *et al.,* 2001).

Sometimes, circulation studies are based on climatologies (e.g. Zhang and Hogg, 1992). Roemmich and Sutton (1998) assess the representativeness of a particular upper-ocean climatology, derived from a large number of repeat measurements. They find that the representativeness depends directly on the number of available samples in a given region. Climatologies that are derived from singly occupied hydrographic sections are, therefore, not any more representative of the mean state than the individual sections from which they are constructed.

The primary goal of the present study is an assessment of the representativeness of the geostrophic shear observed in three modern meridional hydrographic sections between 3 and 30S in the western South Atlantic (Brazil Basin). First, we show that tracer fields in the North Atlantic Deep Water (NADW) observed during the WOCE period are consistent with float-derived velocity measurements, implying the existence of a quasi-steady large-scale zonal circulation (Section 2). Visually, the vertical shear calculated from the meridionally filtered hydrographic sections appears to be dominated by the mean zonal flow field. Quantitatively, however, the shear samples are only marginally representative of the mean (Section 3). Instantaneous geostrophic velocities, therefore, describe the mean circulation only qualitatively. The large-scale baroclinic temporal variability is dominated by the lowest two dynamical modes. After these are removed the residuals agree quantitatively, i.e. the filtered samples are representative of the filtered mean. However, the

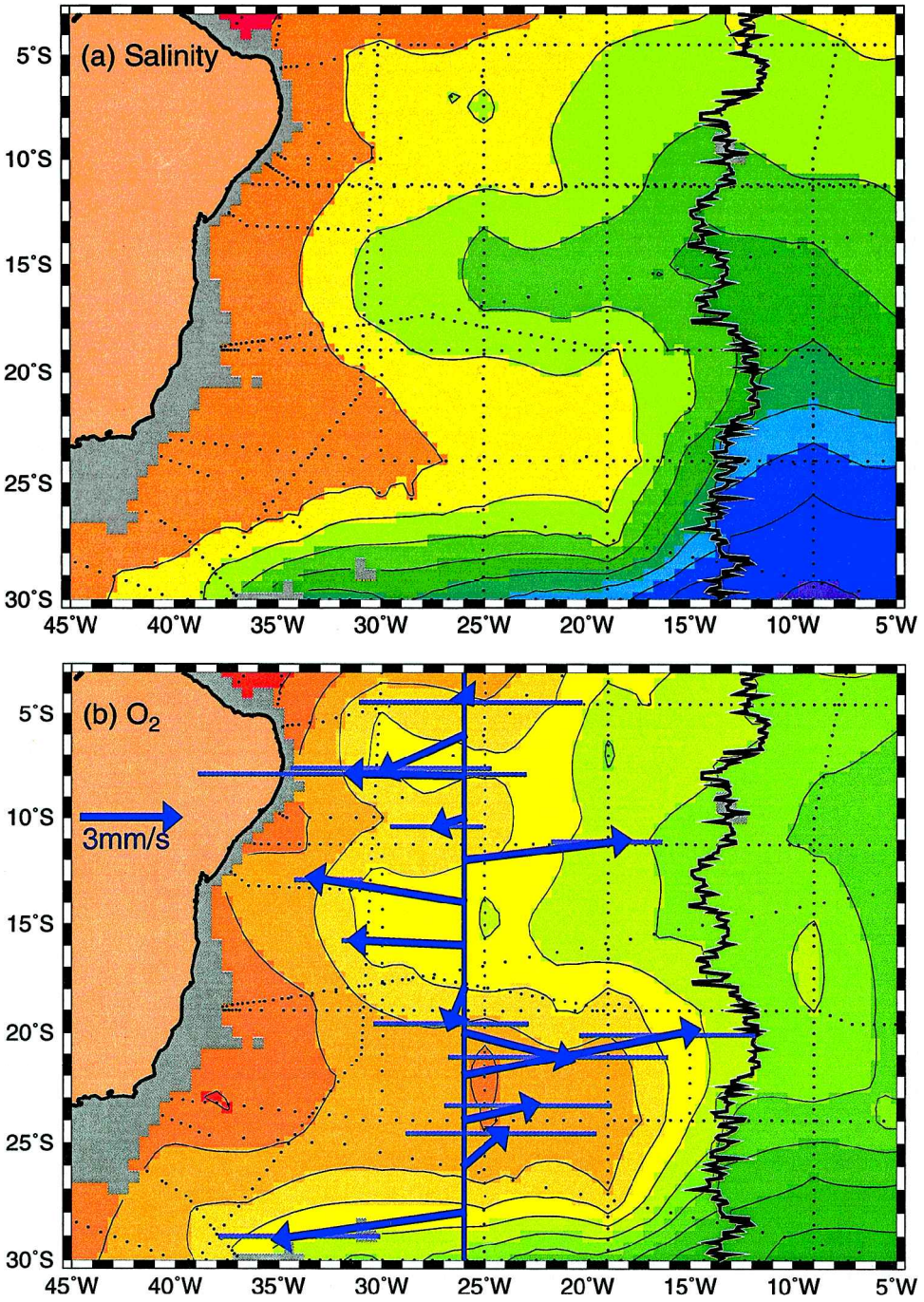

Figure 1. Bias-corrected tracer fields at 2500 m in the Brazil Basin. (a) Salinity (0.01 contour interval). (b) Oxygen (2.5 μmol kg^{-1} contour interval) and spatially averaged (in boxes spanning 2° of latitude by 8° of longitude) float velocities (arrows); zonal-velocity uncertainties are indicated by the horizontal bars at the tips of the arrows; none of the meridional velocities is significantly different from zero (Treguier *et al.,* 2003). (c) Silicate (2 μmol kg^{-1} contour interval) and stations of the three meridional hydrographic sections analyzed in this study; stars indicate the USNS Wilkes stations (see text for details). The crest of the Mid-Atlantic Ridge is shown near 14W.

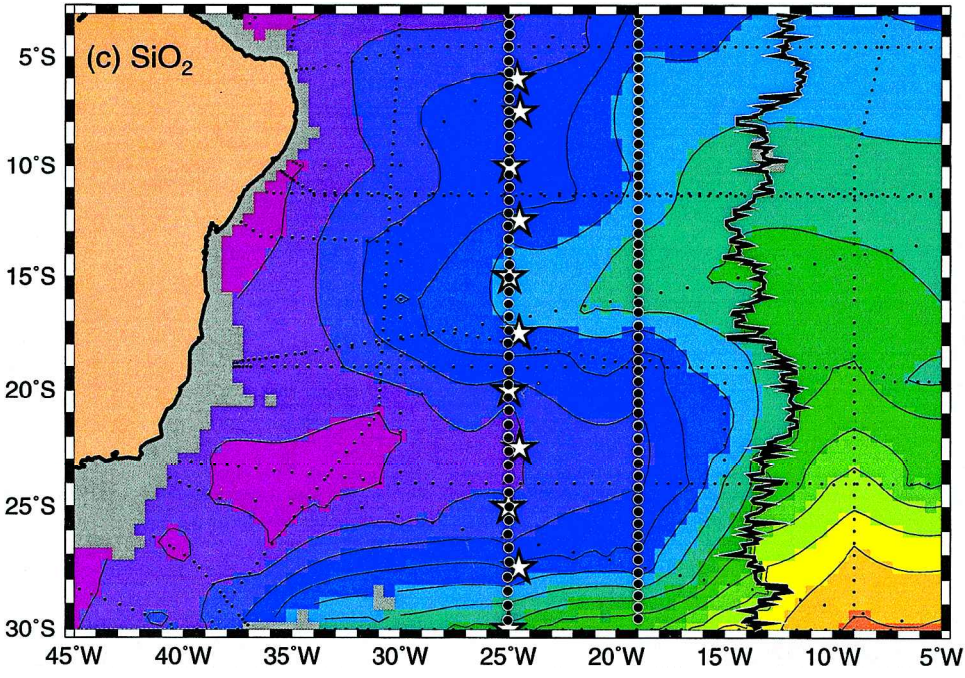

Figure 1. (Continued)

data also indicate that there is significant low-mode energy in the mean flow as well (Section 4). The main results are discussed in Section 5.

2. NADW tracer tongues in the Brazil Basin

At the depth of NADW in the Brazil Basin horizontal maps of bias-corrected tracer data collected between 1983 and 2001 (see Appendix for details) are characterized by several zonal tongues (Fig. 1). Talley and Johnson (1994) and Tsuchiya *et al.* (1994) discuss the property extrema along 25W, which (in the case of Talley and Johnson (1994) by analogy with Pacific tracer distributions) they infer to be zonal tongues. Our tracer maps indicate that the NADW tongues are restricted to the region west of the Mid-Atlantic Ridge. Because the tracer tongues extend across sections occupied in different years, the synoptic samples are representative of a persistent WOCE-decade mean state. At the resolution permitted by the measurement accuracy and station spacing of the 1925–1927 Meteor data (Wüst, 1935), the pattern appears not to have changed significantly during more than half a century.

Between 30W and the crest of the Mid-Atlantic Ridge near 14W there are at least three meridional hydrographic sections between 3 and 30S across the Brazil Basin (Fig. 1c): the WOCE sections A15 at 19W (April/May 1994) and A16 (aka. SAVE 6, aka. Hydros 4) at 25W (March/April 1989), as well as a section nominally at 24.5W constructed from

full-depth stations occupied between March and September 1983 as part of a hydrographic survey carried out on USNS *Wilkes* (Gordon and Bosley, 1991). The meridional station spacing of the Wilkes section (nominally 2.5°) is much coarser than that of the WOCE sections (0.5°). In the deep water the vertical resolution of the Wilkes data is as low as one measurement every 200 dbar; linear interpolation was used to resample the data at 50 dbar intervals. In order to calibrate the Wilkes salinities, the *T/S* properties below 3500 m were adjusted to data from the nearest A16 stations, resulting in corrections up to 0.08 (the nominal WOCE salinity accuracy is 0.002).

Meridional tracer sections corroborate the inference of zonally coherent persistent tracer tongues in the Brazil Basin (Fig. 2). The tracer "anomalies" below 1000 m near 19S in the 19W section are caused by an eddy pair (Weatherly *et al.,* 2002), and the corresponding stations were removed from the A15 data. In contrast to the layers above and below, there is significant meridional and vertical tracer structure in the NADW occupying the approximate depth range between 1500 and 4000 m. Both the meridional and the vertical scales of the tracer tongues decrease toward the equator. At low latitudes the tongues are not well resolved in the Wilkes section.

In the NADW the mean flow derived from float trajectories (Hogg and Owens, 1999) is primarily along the axes of the tracer tongues (Figs. 1b and 2), supporting the central assumption of Wüst's (1935) core-layer method. For the case of the large NADW tongue centered near 22S, Vanicek and Siedler (2002) reach a similar conclusion using a box-inverse model constrained by conservation of a variety of tracers. At low latitudes, where the scales of the tracer tongues are smaller, the correspondence between the tracer cores and the velocity extrema is less clear. This may be related to insufficient meridional sampling by the floats.

In a steady state, the concentration c of a tracer at a fixed location in the ocean is maintained by a balance of advection, eddy diffusion and internal sources and sinks, i.e.

$$\mathbf{u} \cdot \nabla c = k^{(x)} c_{xx} + k^{(y)} c_{yy} + k^{(z)} c_{zz} - S \tag{1}$$

where $\mathbf{u} = (u\ v\ w)$ is the 3-dimensional velocity vector, $\mathbf{k} = (k^{(x)}\ k^{(y)}\ k^{(z)})$ is the anisotropic austausch or eddy-diffusion coefficient, and S combines the source and sink terms. The right-hand side of expression (1) accounts for the nonconservative processes which introduce spatial variability in the concentrations of dissolved and particulate tracers. Persistent large-scale tracer tongues are often interpreted as evidence for a quasi-steady circulation, but they can be maintained in principle without Eulerian mean flows ($\mathbf{u} = 0$), i.e. by eddy fluxes balancing the sources and sinks (Wunsch, 2001). The float observations, indicating mean flow down the NADW tracer tongues, imply that the deep tracer fields in the Brazil Basin are maintained by advective-diffusive balances, however.

In order to gain a quantitative understanding of the dominant balance maintaining the tracer tongues, the terms of expression (1) are evaluated with data from the high-NADW tongue centered at 22S and from the low-NADW tongue centered at 15S. In the cores of

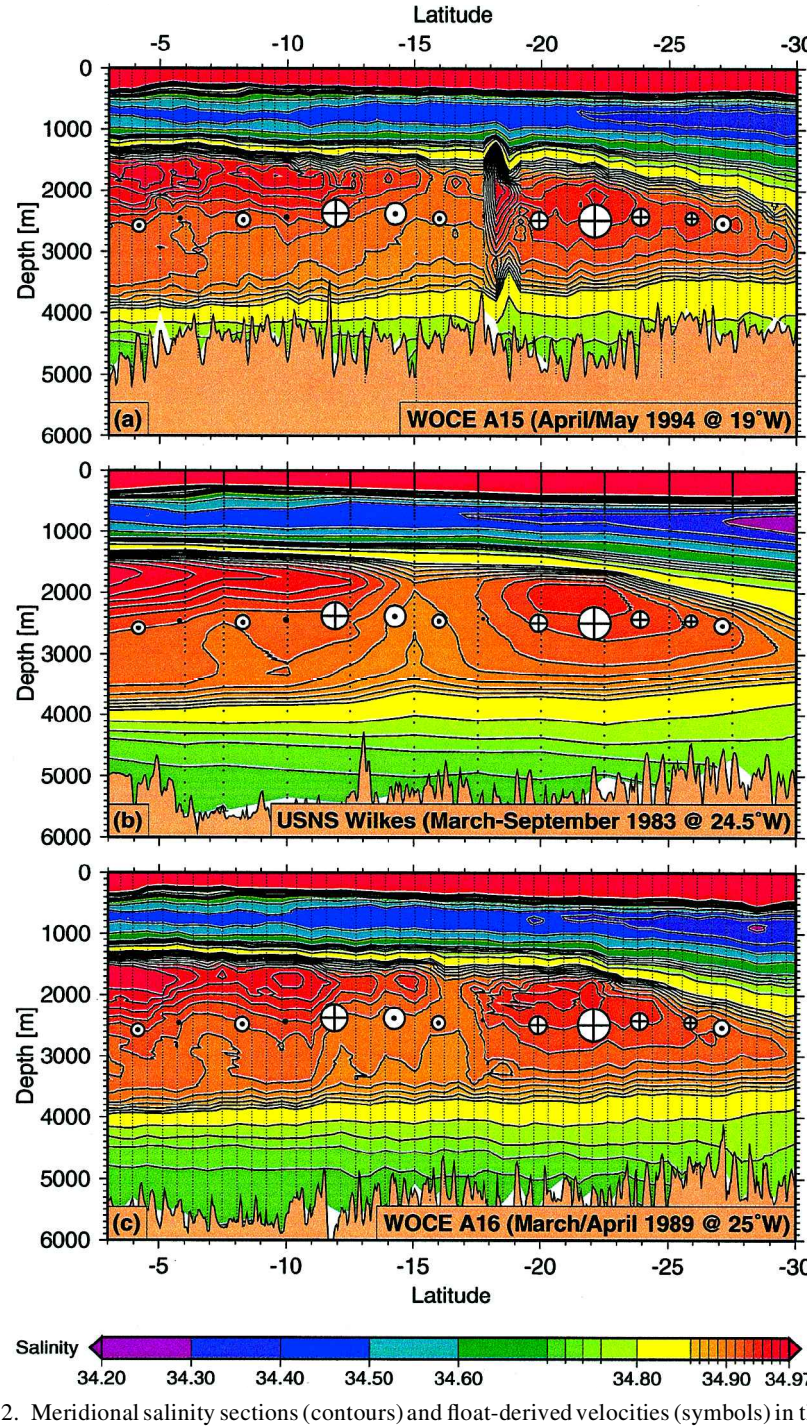

Figure 2. Meridional salinity sections (contours) and float-derived velocities (symbols) in the Brazil Basin; see Figure 1c for station positions. The areas of the symbols are proportional to the float-derived speeds.

Table 1. Advective-diffusive balances in the NADW tracer tongues centered at 15° and 22S; see text for details.

Property tongue	c_x	c_{yy}	$k^{(y)}$
15S salinity	$-1.4(\pm0.1)\times10^{-8}\,\mathrm{m^{-1}}$	$1.0(\pm0.3)\times10^{-13}\,\mathrm{m^{-2}}$	$700\,\mathrm{m^2\,s^{-1}}$
15S oxygen	$-3.9(\pm0.2)\times10^{-6}\,\mu\mathrm{mol\,kg^{-1}\,m^{-1}}$	$3.8(\pm1.2)\times10^{-11}\,\mu\mathrm{mol\,kg^{-1}\,m^{-2}}$	$513\,\mathrm{m^2\,s^{-1}}$
15S silicate	$4.8(\pm0.3)\times10^{-6}\,\mu\mathrm{mol\,kg^{-1}\,m^{-1}}$	$-2.8(\pm1.3)\times10^{-11}\,\mu\mathrm{mol\,kg^{-1}\,m^{-2}}$	$857\,\mathrm{m^2\,s^{-1}}$
22S salinity	$-9.9(\pm1.2)\times10^{-9}\,\mathrm{m^{-1}}$	$-4.7(\pm1.4)\times10^{-14}\,\mathrm{m^{-2}}$	$1053\,\mathrm{m^2\,s^{-1}}$
22S oxygen	$-2.1(\pm0.4)\times10^{-6}\,\mu\mathrm{mol\,kg^{-1}\,m^{-1}}$	$-1.6(\pm0.6)\times10^{-11}\,\mu\mathrm{mol\,kg^{-1}\,m^{-2}}$	$656\,\mathrm{m^2\,s^{-1}}$
22S silicate	$3.2(\pm0.2)\times10^{-6}\,\mu\mathrm{mol\,kg^{-1}\,m^{-1}}$	$1.5(\pm0.6)\times10^{-11}\,\mu\mathrm{mol\,kg^{-1}\,m^{-2}}$	$1067\,\mathrm{m^2\,s^{-1}}$

these tongues meridional tracer advection can be ignored because of the dominance of the zonal velocities, and because the meridional tracer gradients vanish there. The curvature terms, which imply nonzero eddy-diffusive fluxes, are evaluated from quadratic fits to the observed tracer fields. The horizontal maps suggest that west of ≈18W there is little zonal curvature in the NADW tracer fields (Fig. 1); a quadratic fit to the salinities between 18 and 35W at 2500 m in a 24S section yields $c_{xx} = 1.0(\pm2.1)\times10^{-15}\,\mathrm{m^{-2}}$. The meridional curvatures in the 25W section at 11–18S and at 18–26S are two orders of magnitude larger ($c_{yy} = 1.0(\pm0.3)\times10^{-13}\,\mathrm{m^{-2}}$ and $c_{yy} = -4.7(\pm1.4)\times10^{-14}\,\mathrm{m^{-2}}$, respectively), confirming the visual impression. The ratio of the integral time scales of the zonal and meridional velocities in this region is approximately 2 (Hogg and Owens, 1999), implying that $k^{(x)}$ and $k^{(y)}$ are of the same order. The small zonal curvature in the salinity field therefore implies that zonal eddy diffusion can be ignored. The vertical curvature of salinity in the NADW layer (1500–4000 m) at 25W/24S is $c_{zz} \approx 10^{-7}\,\mathrm{m^{-2}}$. In conjunction with an estimate of the vertical eddy diffusivity at 2500 m in the Brazil Basin west of 18W ($\approx2\text{–}3\times10^{-5}\,\mathrm{m^2\,s^{-1}}$; from Fig. 2 of Polzin *et al.,* 1997) this implies that the vertical component of eddy diffusion can be ignored as well, as long as $k^{(y)} \gg 20\,\mathrm{m^2\,s^{-1}}$. With these scales, expression (1) applied to conservative tracers ($S = 0$) simplifies to a balance between zonal advection and meridional eddy diffusion, i.e.

$$uc_x = k^{(y)}c_{yy}. \tag{2}$$

The float trajectories indicate zonal-flow speeds $|u| \approx 5\times10^{-3}\,\mathrm{m\,s^{-1}}$, both at 15S and at 22S (Fig. 1b). The zonal tracer gradients c_x are evaluated from the gridded climatology (see Appendix for details) at 15 and 22S. The meridional tracer curvatures c_{yy} are calculated from quadratic fits to the data in the 25W section in the latitude ranges 11–18S and 18–26S. Using the resulting estimates in expression (2) yields meridional eddy diffusivities between 500 and 1000 $\mathrm{m^2\,s^{-1}}$ (Table 1). These values are consistent with a meridional-eddy-diffusivity scale of $\approx250\,\mathrm{m^2\,s^{-1}}$, estimated from the eddy-kinetic energy ($1.5\times10^{-4}\,\mathrm{m^2\,s^{-2}}$) and the integral time scale of the meridional velocities (20 days) in this region (Hogg and Owens, 1999). So far we have only shown that expression (2) is a valid approximation for the salinity tongue at 22S—the generally good agreement of the meridional eddy diffusivities derived from oxygen and silicate data (Table 1) suggests that

the approximation holds for these nonconservative tracers as well. The zonal gradients and meridional curvatures in the tracer fields at 15S are significantly larger than the corresponding values in the 22S tongue, but they yield similar meridional eddy diffusivities (Table 1). A balance between meridional eddy diffusion and zonal advection in the tracer tongues at the depth of the NADW in the Brazil Basin is, therefore, a consistent and plausible steady state.

3. Representativeness of synoptic density gradients

The NADW tracer and float data in the Brazil Basin are consistent with meridionally alternating zonal flows with equatorward-decreasing spatial scales (Section 2). This is largely inconsistent with circulation schemes derived from analyses of hydrographic data (e.g. Reid, 1989; DeMadron and Weatherly, 1994). Nevertheless, flow in the correct directions in the vicinity of the largest zonal tracer tongues near 15 and 25S is part of most inferred circulations. Below, we show that these two observations are consistent with the hydrographic snapshots being marginally representative of the mean.

In order to determine zonal geostrophic velocity profiles from hydrographic data the vertical shear calculated from meridional density gradients is integrated. The thermal wind equation is

$$u_z = \frac{g}{f_{\rho_0}} \rho_y, \tag{3}$$

where u_z is the vertical shear of the geostrophic zonal velocity, g is the acceleration due to gravity, f is the Coriolis frequency, ρ_0 is a reference density, and ρ_y is the meridional gradient of density. In order to remove the effects of mesoscale eddies and internal waves ρ_y is estimated from linear fits in meridional windows that are much wider than the first baroclinic Rossby radius. The resulting density gradients are characterized by similar vertical structure over a range of window sizes (Fig. 3a). Furthermore, the gradients at a given latitude are qualitatively similar in the three hydrographic sections (Fig. 3b), suggesting that the vertical structure is a signature of the mean zonal circulation, which is longitudinally coherent between 19 and 25W.

The similarity between the three available meridional-density-gradient samples (with different spatial resolutions) is striking and extends over the entire latitude band covered by all three hydrographic sections (Fig. 4). The main qualitative differences occur near the southern and northern limits of the sections where the windows used for the gradient calculations are truncated. There are no indications that the 24.5 and 25W sections are any more similar to each other than to the 19W section (see also Fig. 3b). Therefore, we will ignore the zonal separation and treat the data as three temporal snapshots of the same field. (This is discussed further in Section 5.) The visual similarity between the three density-gradient snapshots is largely determined by the locations of the zero crossings. The thermal wind equation (3) implies that zero

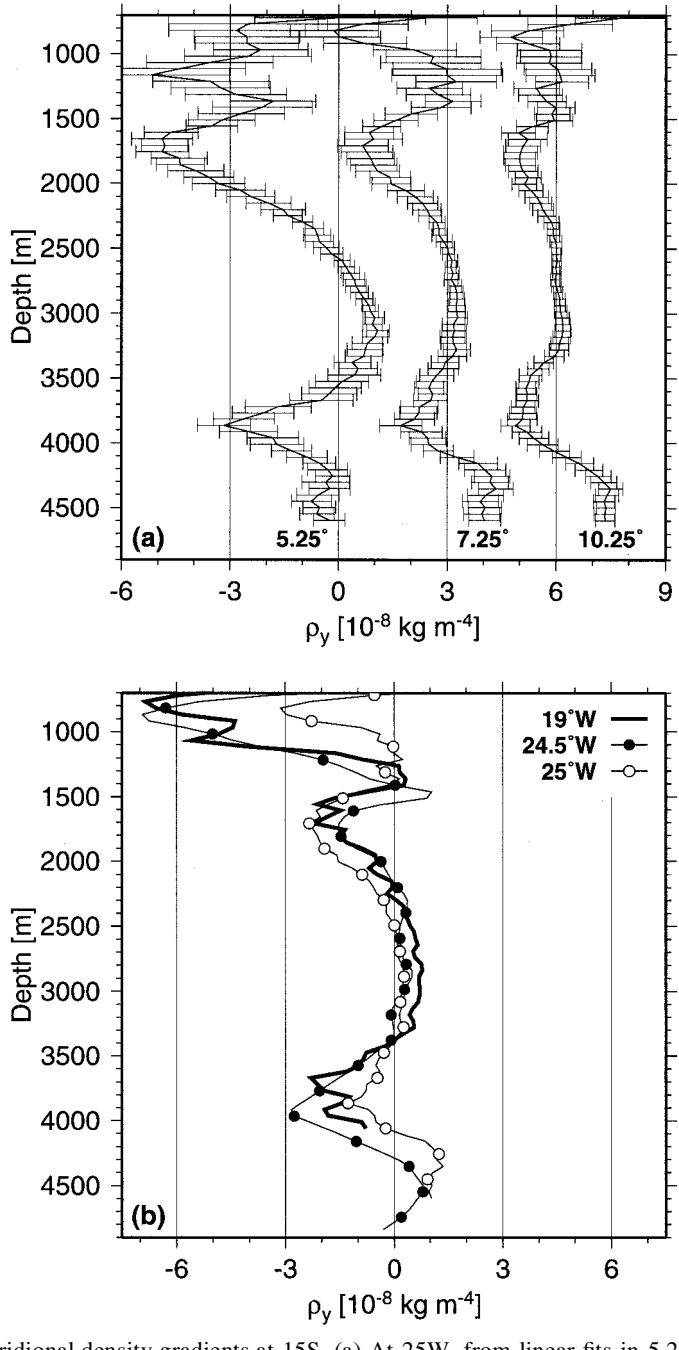

Figure 3. Meridional density gradients at 15S. (a) At 25W, from linear fits in 5.25°-, 7.25°- and 10.25°-wide meridional windows. (b) At 19, 24.5 and 25W, from linear fits in 7.25-wide meridional windows.

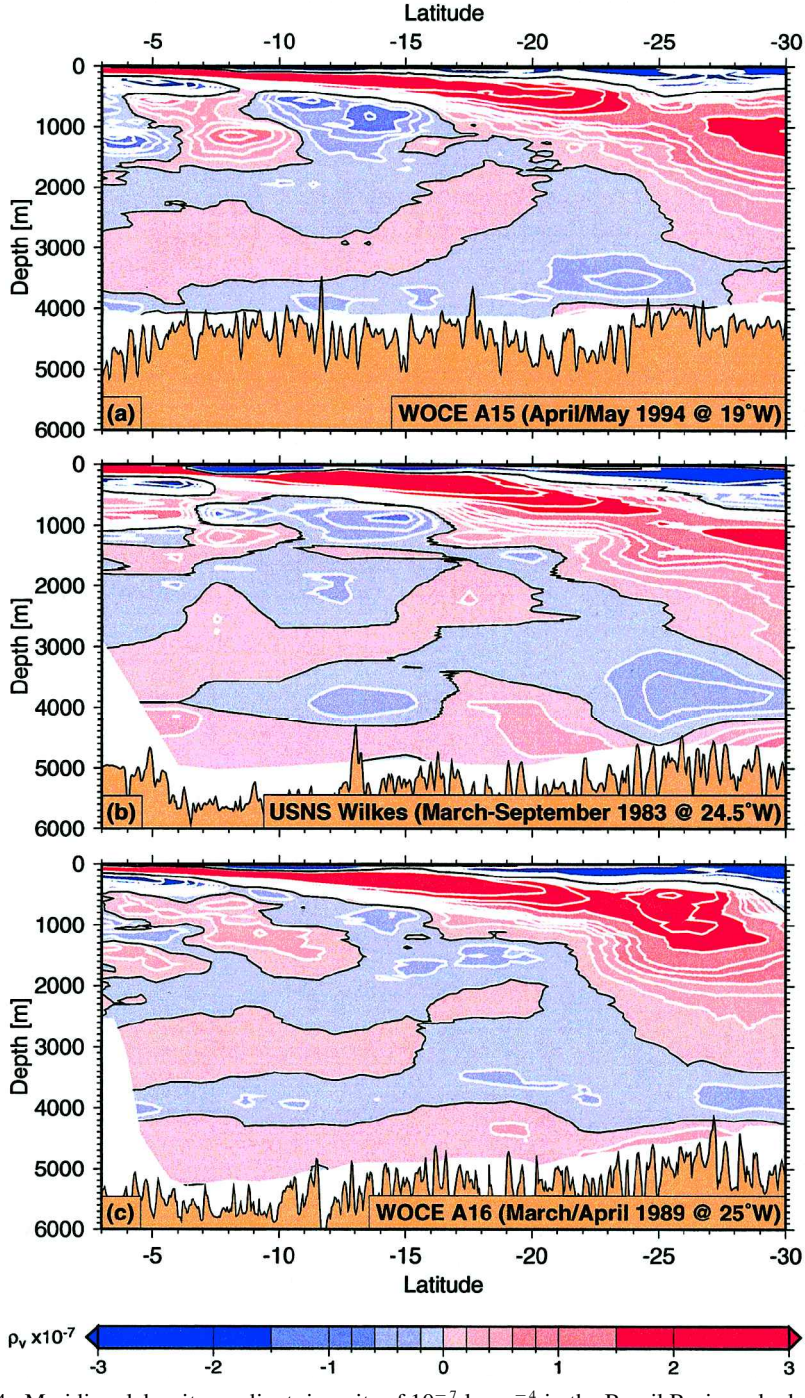

Figure 4. Meridional density gradients in units of 10^{-7} kg m^{-4} in the Brazil Basin, calculated from linear fits in 7.25°-wide meridional windows.

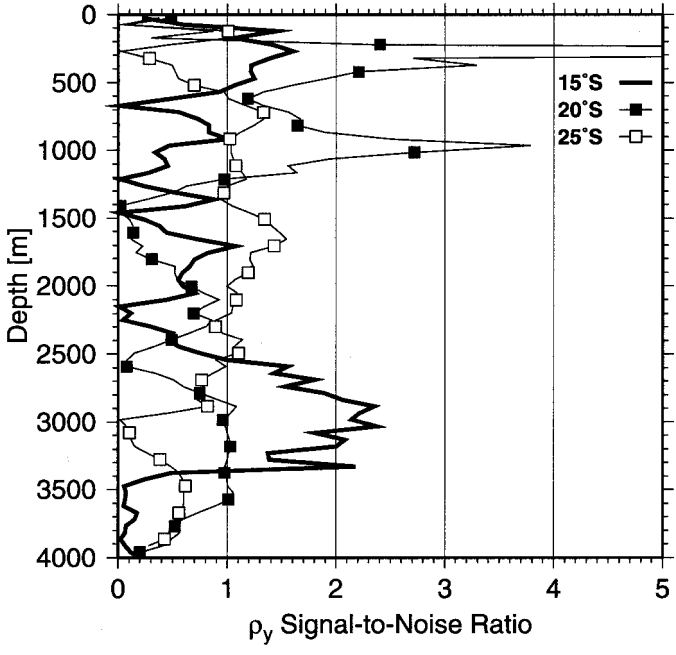

Figure 5. Meridional-density-gradient signal-to-noise ratios, defined as $|\rho_y|/\sigma(\rho_y)$.

crossings in ρ_y correspond to vertical extrema in the zonal geostrophic velocities. Regardless of the fitting window used, there is such a zero crossing (a westward velocity maximum) near 2500 m at 15S (Fig. 3a). Farther south there are additional zonal-velocity extrema near 2500 m between 20 and 25S, consistent with the tracer and float data (Figs. 1 and 2).

In order to assess the representativeness of the individual hydrographic snapshots quantitatively, a signal-to-noise ratio is defined from the magnitude of the sample mean density gradient and the corresponding standard deviation ($|\rho_y|/\sigma(\rho_y)$), calculated from the three realizations at the latitudes of the Wilkes stations—three examples are shown in Figure 5. Surprisingly (given the qualitative similarities of the density-gradient snapshots) there are only a few isolated peaks where the signal-to-noise ratios are markedly greater than one, i.e. where individual samples of the large-scale density gradients can be considered representative. The largest signal-to-noise ratios (up to 20) occur where the three available density-gradient-profiles intersect, i.e. where the standard deviations nearly vanish. In spite of these peaks of high signal-to-noise ratios, the average over the entire region is only 1.1, indicating marginal representativeness. The mean signal-to-noise ratio remains unchanged when the samples associated with small gradients ($|\rho_y| \leq 5 \times 10^{-9}$ kg m^{-4}) or small standard deviations ($\sigma(\rho_y) \leq 5 \times 10^{-9}$ kg m^{-4}) are excluded.

4. Geostrophic velocities

In order to illustrate the implications of the marginal representativeness of the large-scale meridional density gradients in the Brazil Basin (Section 3) for circulation studies, examples of the geostrophic velocities at 25S are shown in Figure 6. At most latitudes in the Brazil Basin there is little vertical shear in the NADW (Fig. 4); at 25S the region of small gradients is restricted to the layer between 2000 and 3000 m. In this layer, the marginal representativeness does not introduce large errors as long as the profiles are referenced using known NADW velocities (Fig. 6a). On the other hand, the density gradients in this layer do not contribute information—setting $\rho_y = 0$ is as valid as using any of the hydrographic sections. The geostrophic shears above and below the NADW layer are qualitatively consistent, i.e. all three samples show that the currents near the surface and near the sea bed are westward compared to the flow between 2000 and 3000 m. Quantitatively, the uncertainties are of the same magnitude as the signal, however.

In most regions of the deep ocean there are no direct velocity measurements available and an assumption of a deep level-of-no-motion is often made (e.g. DeMadron and Weatherly, 1994; Suga and Talley, 1995). At 25S an assumed level-of-no-motion at 4000 m yields peak eastward NADW velocities between 2 and 7 mm s^{-1} (Fig. 6b). Except for a thin layer around 4000 m the uncertainties are again as high as the signal itself, consistent with marginal representativeness. Warren and Speer (1991) and Speer *et al.* (1995) use a level-of-no-motion at 1300 m to infer the zonal transport of NADW near 22S. In the case of the profile shown in Figure 6, the resulting NADW velocities are eastward with peak speeds between 5 and 12 mm s^{-1}, again consistent with marginal representativeness.

Shallow reference velocities (e.g. from upper-ocean floats, surface drifters, or shipboard velocity measurements) are available in many more regions than deep reference velocities. In order to exclude possible effects of ageostrophic flow near the surface the example shown in Figure 6c is referenced in Antarctic Intermediate Water at 750 m. Of all three examples this illustrates the worst case: the inferred deep velocity field depends even qualitatively on the synoptic sample used. (Only one of the three profiles shows eastward flow.)

The examples shown in Figure 6 make it clear that it is not possible to bring the three hydrographic samples at 25S into agreement by adjusting reference velocities, i.e. the temporal variability is baroclinic. In order to characterize the variability across the entire Brazil Basin, baroclinic zonal velocity differences were calculated from the two WOCE sections (Fig. 7a). The spatial scales and the strength of the temporally varying flow field are similar across the entire Brazil Basin; therefore, the inferences drawn from the profiles at 25S hold across the entire domain.

A modal decomposition of the baroclinic zonal velocity differences, using buoyancy-frequency profiles averaged between 19 and 25W, and over 7° of latitude, reveals that the lowest two dynamical modes account for 90% of the total baroclinic kinetic-energy difference (Fig. 7b). In order to illustrate the quality of the modal decomposition, the first

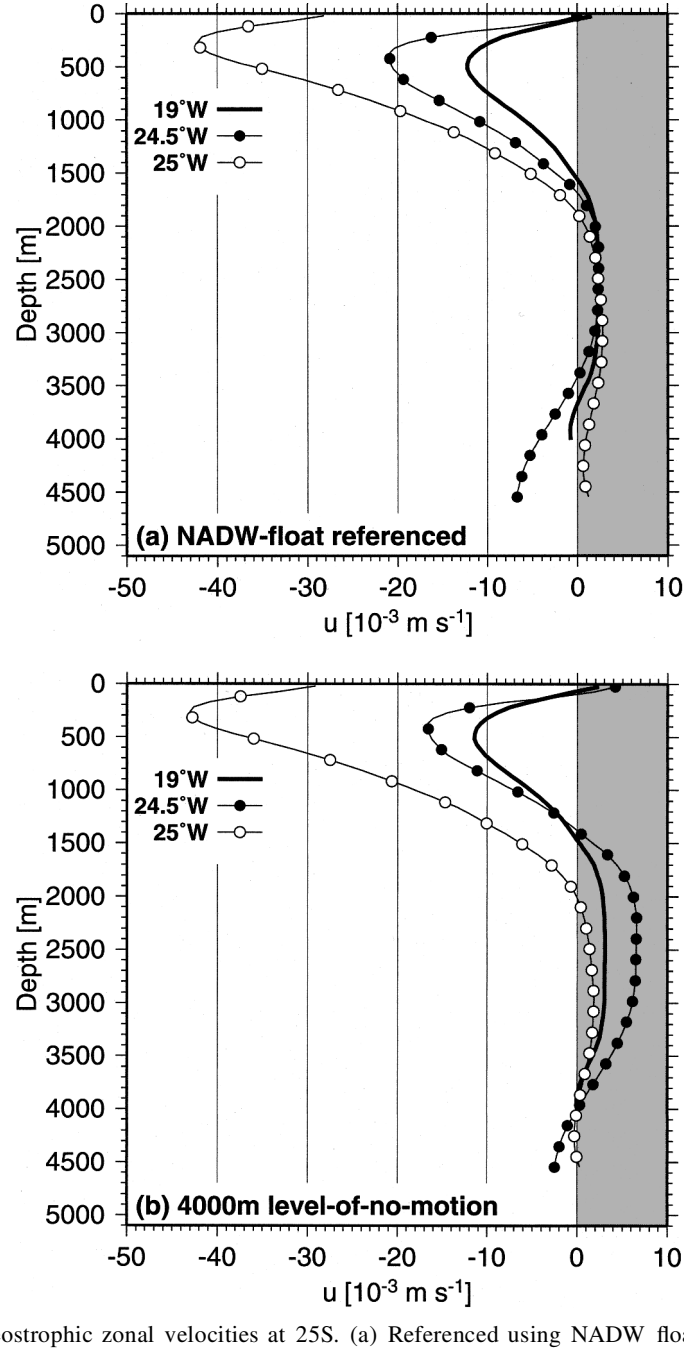

Figure 6. Geostrophic zonal velocities at 25S. (a) Referenced using NADW float data (2.3×10^{-3} m s^{-1} at 2500 m). (b) Assuming a level-of-no-motion at 4000 m. (c) Referenced to a float velocity at 750 m (-20×10^{-3} m s^{-1}, from Richardson and Garzoli (2003)).

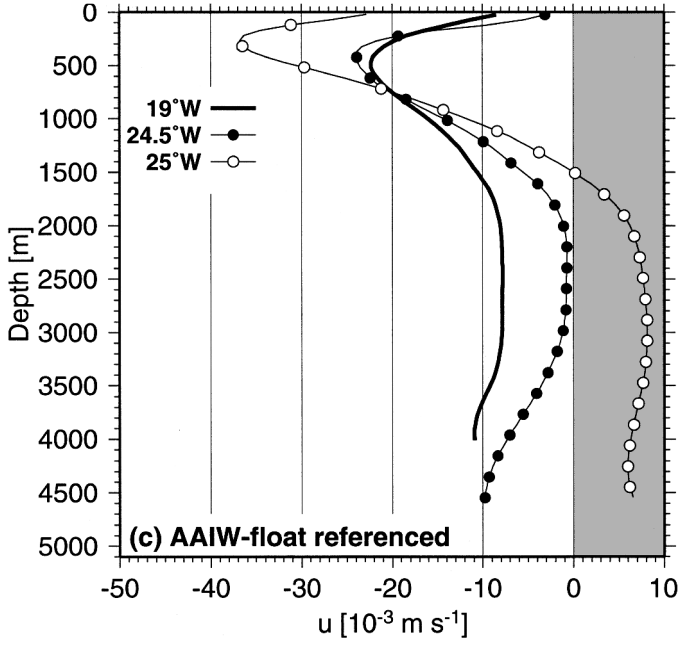

Figure 6. (Continued)

two dynamical modes are shown together with observed baroclinic zonal-velocity differences at 25° and at 23S in Figure 8. (These two latitudes were chosen for their near-perfect fits with the two modes; Fig. 7b.) The largest residuals occur near the surface and near the sea bed. The baroclinic velocity differences between the (spatially nearly coinciding) Wilkes and the WOCE A16 sections are qualitatively (in terms of the horizontal and vertical scales) and quantitatively (in terms of the velocity magnitudes) similar to the ones shown in Figure 7, but the lowest two modes account for only 70% of the total. This may be related to the comparatively coarse spatial resolution of the Wilkes section.

The characteristic meridional scale of the baroclinic velocity differences (≈500 km) is similar to that of the mean deep zonal flows in the Brazil Basin (Section 2), implying that there is no meridional scale separation between the quasi-steady and the temporally varying zonal circulations in the Brazil Basin. The rms zonal-velocity difference at 2500 m is 4.8×10^{-3} m s^{-1}, similar to the rms zonal float velocity of 4.1×10^{-3} m s^{-1}, (calculated from the spatially averaged data). The similar strengths of the large-scale temporally variable and the mean zonal circulations is consistent with the inference of marginal representativeness of the meridional density gradients (Section 3).

The high-mode residual zonal geostrophic velocities that remain after removing the barotropic and the first two baroclinic modes are similar in all three synoptic samples (Fig. 9). The mean signal-to-noise ratio of the corresponding meridional density gradients is 2.3 (vs. 1.1 in the case of the unfiltered density gradients; Section 3), quantitatively

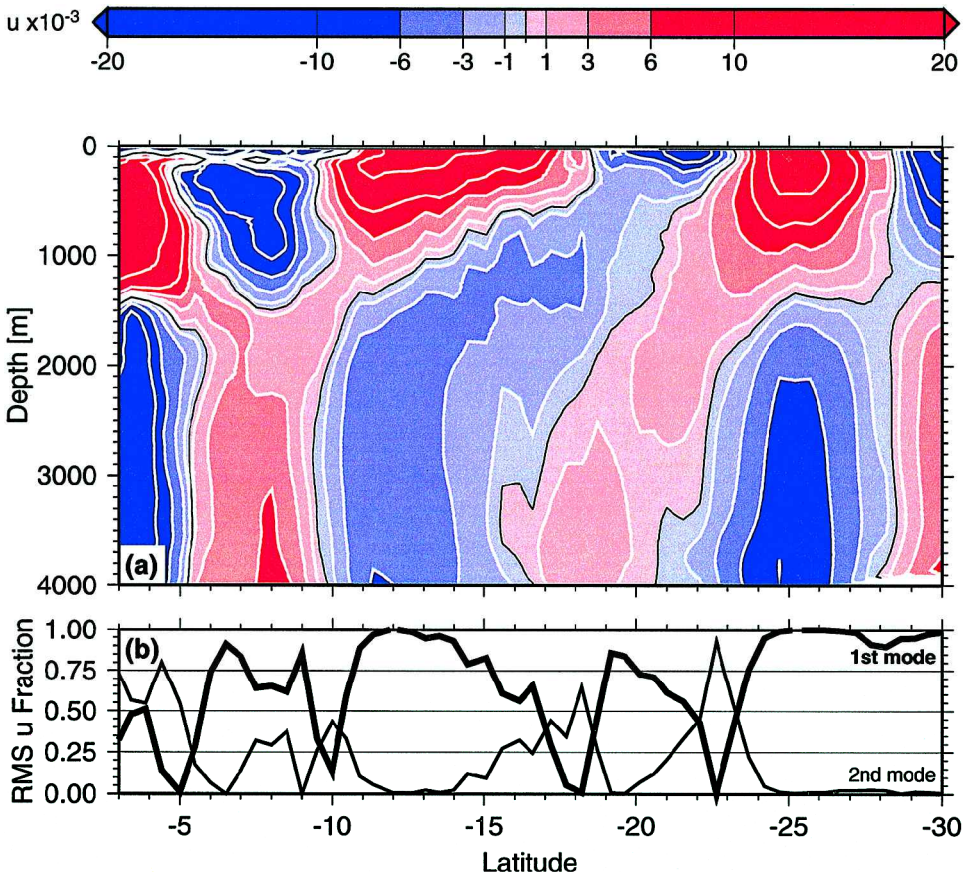

Figure 7. (a) Baroclinic zonal velocity differences between the two WOCE sections (A15 minus A16), in units of 10^{-3} m s^{-1}. (b) Modal decomposition; overall, the first two baroclinic modes account for 90% of the rms velocity difference.

confirming representativeness. The meridional scales of the residual flows are of the same order as those of the NADW tracer tongues, float velocities, and of the temporally varying zonal flows. The residual rms zonal velocity at 2500 m is 1.1×10^{-3} m s^{-1}, i.e. several times smaller than the float-derived rms velocity. Therefore, Figure 9 does not depict the mean zonal circulation in the Brazil Basin. What is missing is the projection of the mean flow onto the barotropic and the first two baroclinic modes.

5. Discussion

Tracer, float and hydrographic data from the Brazil Basin support the concept of a persistent large-scale zonal circulation that can be considered quasi-steady on at least a decadal time scale. At the depth of NADW near 2500 m the mean flow field is dominated

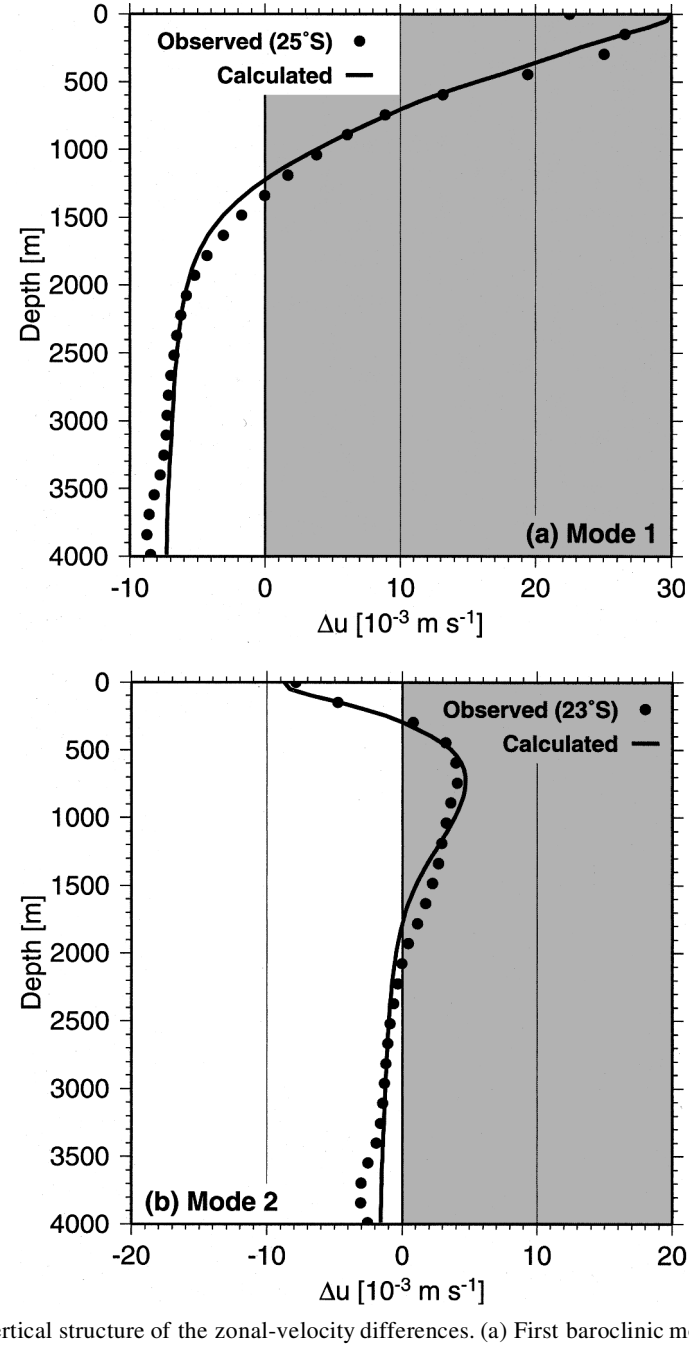

Figure 8. Vertical structure of the zonal-velocity differences. (a) First baroclinic mode at 25S. (b) Second baroclinic mode at 23S.

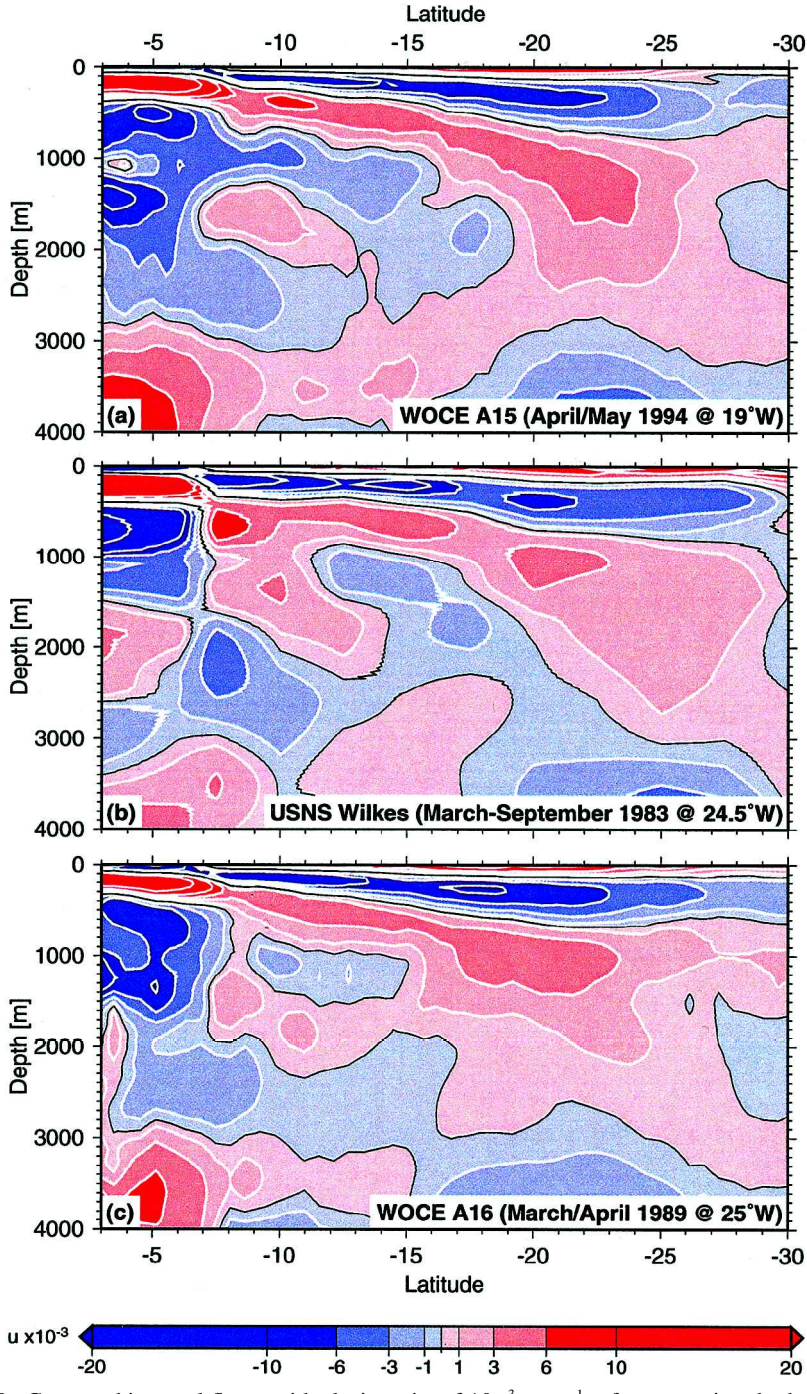

Figure 9. Geostrophic zonal-flow residuals, in units of 10^{-3} m s^{-1}, after removing the barotropic and the first two baroclinic modes.

by meridionally alternating zonal-velocity cores with speeds of a few mm s^{-1}. The close correspondence of the meridional locations of the velocity maxima with the cores of several deep tracer tongues is reminiscent of Wüst's (1935) flow diagrams and provides support for his core-layer method. "Wüstian flow" (downgradient along the axes of tracer tongues) requires a balance of advection and diffusion in order to maintain a steady state. In the case of the NADW tongues in the Brazil Basin, zonal advection and meridional eddy diffusion account for the principal balance in the tracer equation.

The mean zonal circulation in the Brazil Basin dominates the pattern of the large-scale meridional density gradients in three quasi-synoptic hydrographic surveys taken between 1983 and 1994. A quantitative comparison shows, however, that the visual similarity between the synoptic snapshots is misleading, as the large-scale variability in the geostrophic shear is of the same order as the shear itself. The observed variability is primarily temporal, rather than spatial, because the similarities between the two WOCE sections (separated by 6° of longitude) are as close as those between the WOCE A16 and the Wilkes sections (separated by $<1°$ of longitude), both in terms of the qualitative density-gradient patterns, and in terms of the modal structure and the magnitudes of the baroclinic zonal-velocity differences. In the case of the large-scale zonal flows in the Brazil Basin the baroclinic temporal variability is dominated by the lowest two dynamical modes. (While this is similar to observations from long-term current-meter records (e.g. Müller and Siedler, 1992; Wunsch, 1997), this result was not anticipated because our spatial averaging removes the small scales, which dominate the variability of velocity point measurements.) It follows that, regardless of the reference velocities used, any zonal circulation scheme derived from synoptic geostrophic shear in the Brazil Basin is only marginally representative and reflects the mean state at best qualitatively.

The magnitudes of the transport errors arising from the marginal representativeness of synoptic density gradients depend on the reference levels and and reference velocities used because the velocity uncertainty at a given depth is comparable in magnitude to the total shear between the reference level and this depth. The total shear between NADW and Antarctic Intermediate Water, for example, is a few cm s^{-1}, implying velocity uncertainties an order of magnitude above the mean-flow velocities in the deep water when geostrophic profiles are referenced to Antarctic Intermediate Water velocities. In the case of surface-referencing, e.g. using shipboard ADCP data or surface drifters, the uncertainties are even larger. The small magnitude of the mid-depth meridional density gradients in the Brazil Basin, on the other hand, implies that the deep-water transport errors are small when reference velocities in the same layer are used. In this case the transport estimates are almost entirely determined by the reference velocities, i.e. the hydrographic data do not contribute significant information. Estimates of the shallow zonal circulation in the Brazil Basin derived from deep reference levels will also be associated with uncertainties of order 100%. This is consistent with results in other regions (e.g. Roemmich and Wunsch, 1985; Armi and Stommel, 1983), suggesting that the marginal representativeness of the Brazil Basin sections is likely to be the rule rather than the exception. On the scales investigated

here, there are no indications for a (meridional) scale separation between the mean flow and the temporal variability, precluding the use of meridional averaging to increase the representativeness.

These observations have potentially serious implications for the dynamic method, box-inverse models as well as β-spirals, because they imply that methods that allow only for barotropic adjustments, and therefore assume that the horizontal density gradients are representative, are fundamentally inconsistent with the Brazil Basin data, regardless of the horizontal averaging scale used. In the case of box-inverse models, the inconsistency can be reduced by relaxing the imposed constraints. Using initial deep reference levels and allowing for comparatively large thermocline mass and tracer imbalances, for example, effectively allows for low-mode variability.

The small magnitude of the high-mode quasi-steady residual baroclinic velocities, when compared to the float data, suggests that there is significant energy in the projection of the mean zonal flow field in the Brazil Basin onto the barotropic and the lowest two baroclinic modes. In order to complete a quantitative determination of the mean zonal circulation in the Brazil Basin (and, presumably, elsewhere) this projection must be determined. Repeat hydrographic profiles in the upper 1000 m or so (because of the vertical structure of the low dynamical modes full-depth profiles are not required) may be the most cost-effective method for attaining that goal, especially if autonomous platforms are used (e.g. Sherman *et al.,* 2001). Once representative geostrophic shear profiles have been determined, it should be possible to solve for the barotropic flows using conventional methods, such as box-inverse models.

Acknowledgments. We thank the contributors of the observational data sets used in this study. The analysis was carried out in the context of the WOCE AIMS Deep Basin Experiment Synthesis project (NSF grants OCE-9911148 and OCE-0220407).

APPENDIX

Bias-corrected tracer and hydrographic climatology of the tropical and subtropical South Atlantic

a. Bias correction

In order to relate tracer patterns to the large-scale circulation, climatological tracer fields are required. The World Ocean Data Base (2001 version; WOD01) contains perhaps the largest collection of hydrographic and tracer data. After discarding the measurements that fail any of the NODC quality checks (see http://www.nodc.noaa.gov for details), almost all remaining data are derived from a small number of WOCE-era hydrographic sections (Fig. 10a). Many of the stations of these sections are rejected by the NODC quality control, resulting in large areas without any data. Therefore, we decided to inspect data from hydrographic sections of known provenance, collected between 1983 and 2001 (Table 2). Most of the sections are publicly available and included in the WOD01. The WOCE A11 and the SAVE 5 sections lie almost entirely outside our study region but are included to

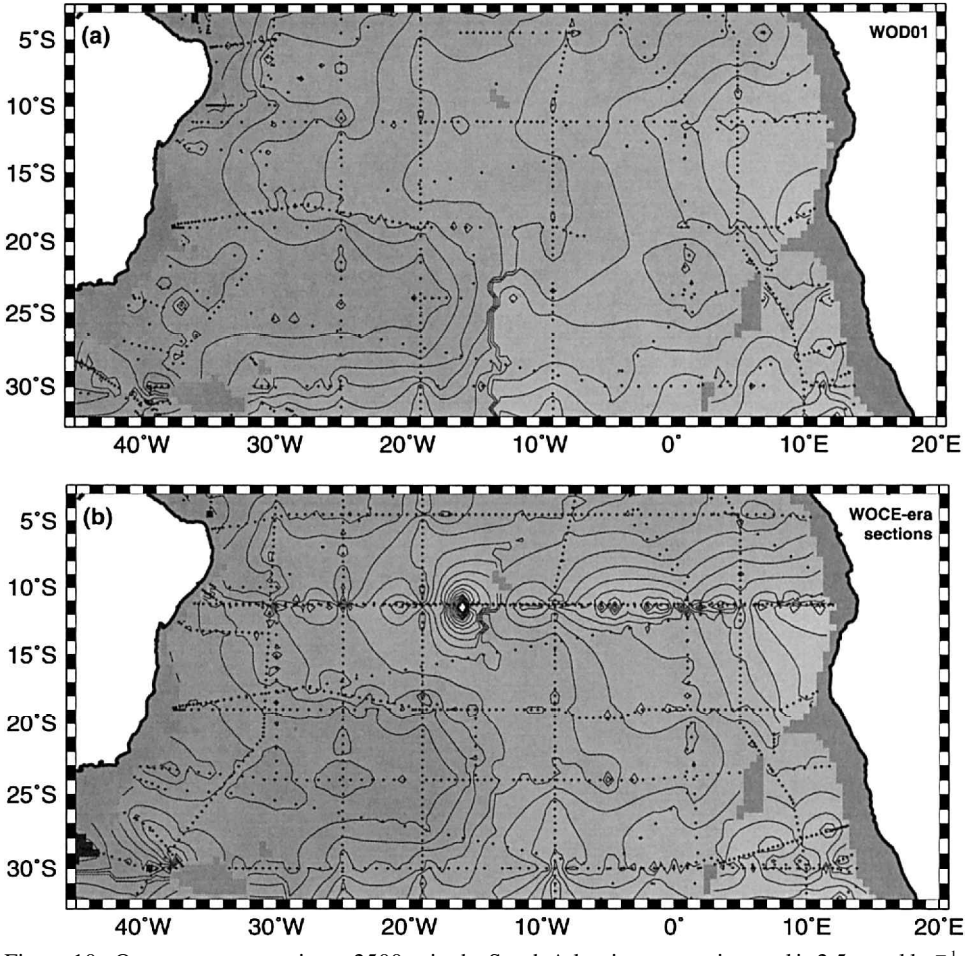

Figure 10. Oxygen concentration at 2500 m in the South Atlantic; contour interval is 2.5 μmol kg^{-1}. (a) NODC-quality-controlled WOD01 data (as of July 24, 2003). (b) Raw data from the hydrographic sections listed in Table 2.

provide additional repeat-sampling regions for calculation of the bias corrections (see below). Inspection of the uncorrected deep oxygen data (Fig. 10b) reveals strong anomalies along 11S caused by bad data in the WOCE A08 section. A detailed comparison with an older section along 11S (Oceanus 133) and with meridional sections at crossovers reveals that the errors in the A08 oxygen data are inconsistent with a single measurement bias. There are similar consistency problems with the silicate and oxygen data of the Discovery 1987 section near the African continent between 27 and 30S. Bad data from these sections were excluded from the climatology.

Many salinity and tracer sections suffer from measurement bias, which can be corrected by considering data from regions that are covered by multiple data sets (usually section

Table 2. Data sets used in the hydrographic and tracer climatology of the South Atlantic.

Data Set	Dates	O_2 Data	SiO_2 Data	Data source
WOCE A07	Jan–Feb 1993	CTD	bottle	WHPO
WOCE A08	Mar–May 1994	bad	bottle	WHPO
WOCE A09	Feb–Mar 1991	CTD	bottle	WHPO
WOCE A10	Jan 1993	CTD	bottle	WHPO
WOCE A11	Dec 1992–Jan 1993	CTD	bottle	WHPO
WOCE A13	Feb–Mar 1995	CTD	bottle	WHPO
WOCE A14	Jan–Feb 1995	CTD	bottle	WHPO
WOCE A15	Apr–May 1994	CTD	bottle	WHPO
WOCE AR15	Apr 1994	CTD	bottle	WHPO
WOCE A16	Mar–Apr 1989	CTD	bottle	WHPO
WOCE A17	Jan–Mar 1994	CTD	bottle	WHPO
WOCE A23	Mar–May 1995	bottle	bottle	WHPO
AJAX 1	Oct–Nov 1983	bottle	bottle	L. Talley
BEST 2	May–Jun 1993	CTD	n/a	A. Gordon
Discovery 1987	Apr–May 1987	bad	bad	A. Gordon
Oceanus 133 (11S)	Mar–Apr 1983	CTD	bottle	M. McCartney
Oceanus 133 (24S)	Feb–Mar 1983	bottle	bottle	M. McCartney
Oceanus 133 (30W)	Feb 1983	bottle	bottle	M. McCartney
SAVE 1	Nov–Dec 1987	CTD	bottle	L. Talley
SAVE 2	Dec 1987–Jan 1988	CTD	bottle	L. Talley
SAVE 3	Jan–Mar 1988	CTD	bottle	L. Talley
SAVE 4	Dec 1988–Jan 1989	CTD	bottle	L. Talley
SAVE 5	Jan–Mar 1989	CTD	bottle	L. Talley
James Clark Ross 65	Sep–Oct 2001	n/a	n/a	C. German
Meteor 41/3	Apr–May 1998	n/a	n/a	W. Zenk
Romanche 2	Nov 1992	CTD	n/a	H. Mercier

crossovers; e.g. Johnson *et al.,* 2001; Gouretski and Jancke, 2001). Gouretski and Jancke (2001) list bias corrections for most of the available data in our study region. Unfortunately, there are still problems in their corrected deep tracer fields (Fig. 11a). The corrected A09 oxygen concentrations at 19S in particular are consistently biased high in comparison with the corresponding values in crossover sections. Furthermore, Gouretski and Jancke (2001) use the bad A08 oxygen data in the global adjustment, which may introduce errors elsewhere. Finally, the Gouretski and Jancke (2001) climatology does not contain the Oceanus 133 sections along 24S and along 30W in the largest of the NADW tracer tongues in the Brazil Basin, and it also lacks some other tracer sections (e.g. AJAX 1 oxygen and silicate, and BEST 2 oxygen). Therefore, we decided to calculate our own bias corrections, using a method similar to the weighted least squares of Johnson *et al.* (2001).

The hydrographic sections listed in Table 2 define 123 repeat-sampling regions with minimum station distances less than 150 km. In each repeat-sampling region all stations within $3° \times 3°$ squares centered at the nearest-neighbor stations of both sections were selected and the deep tracer measurements plotted against potential temperature. This is

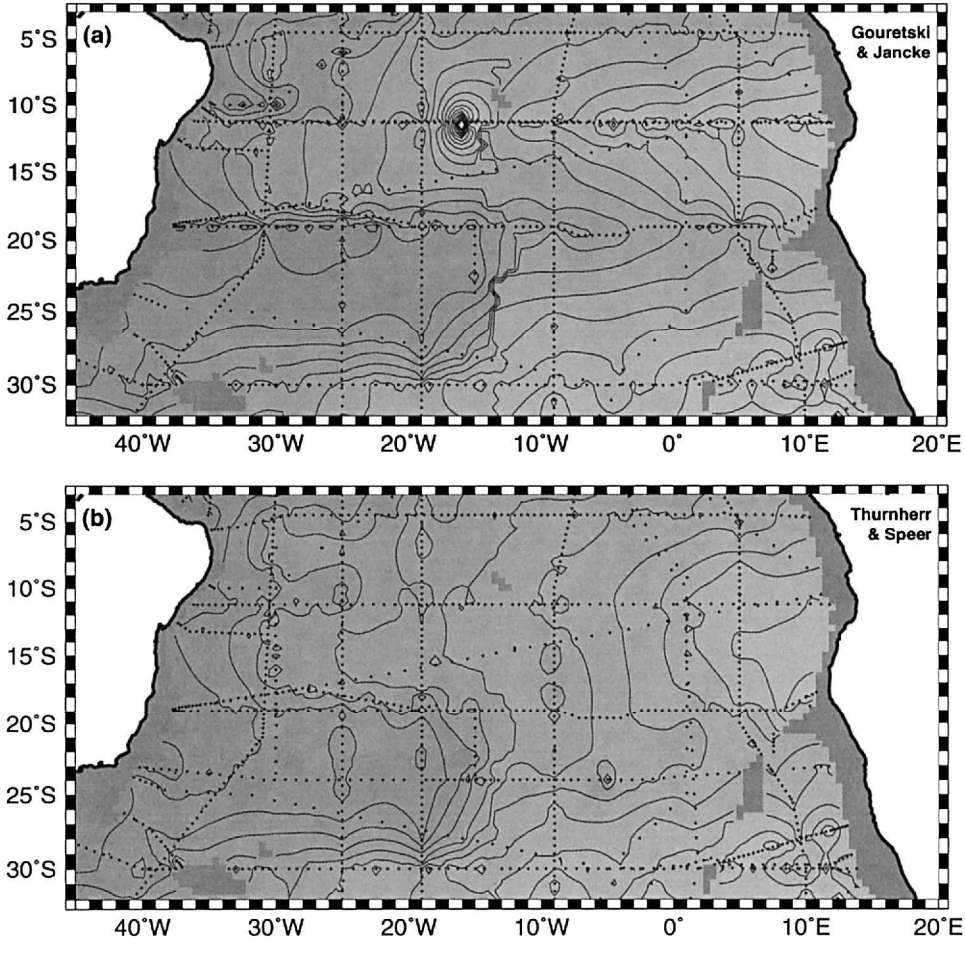

Figure 11. Bias-corrected oxygen concentration at 2500 m in the South Atlantic; contour interval is 2.5 μmol kg^{-1}. (a) Climatology of Gouretski and Jancke (2001). (b) Climatology constructed for this study.

illustrated in Figure 12a with oxygen data from the WOCE A10/A16 section crossover at 30S/25W. For section pairs with multiple repeat-sampling regions the one with the tightest deep tracer envelopes (usually the one extending to the highest density) was chosen. After removal of bad bottle data, temperature ranges for the bias adjustments were chosen manually from each tracer plot. In addition to requiring small scatter within a given section ($\approx$5 μmol kg^{-1} for oxygen, $\approx$3.5 μmol kg^{-1} for silicate, $\approx 3 \times 10^{-3}$ for salinity), regions of significant curvature in potential-temperature space were excluded. The very deepest (coldest) part of the profiles were usually excluded as well, because of the reduced number of profiles there and because there are often "hooks" at the bottom of the tracer profiles (Fig. 12). Repeat-sampling regions without a potential-temperature range spanning at least

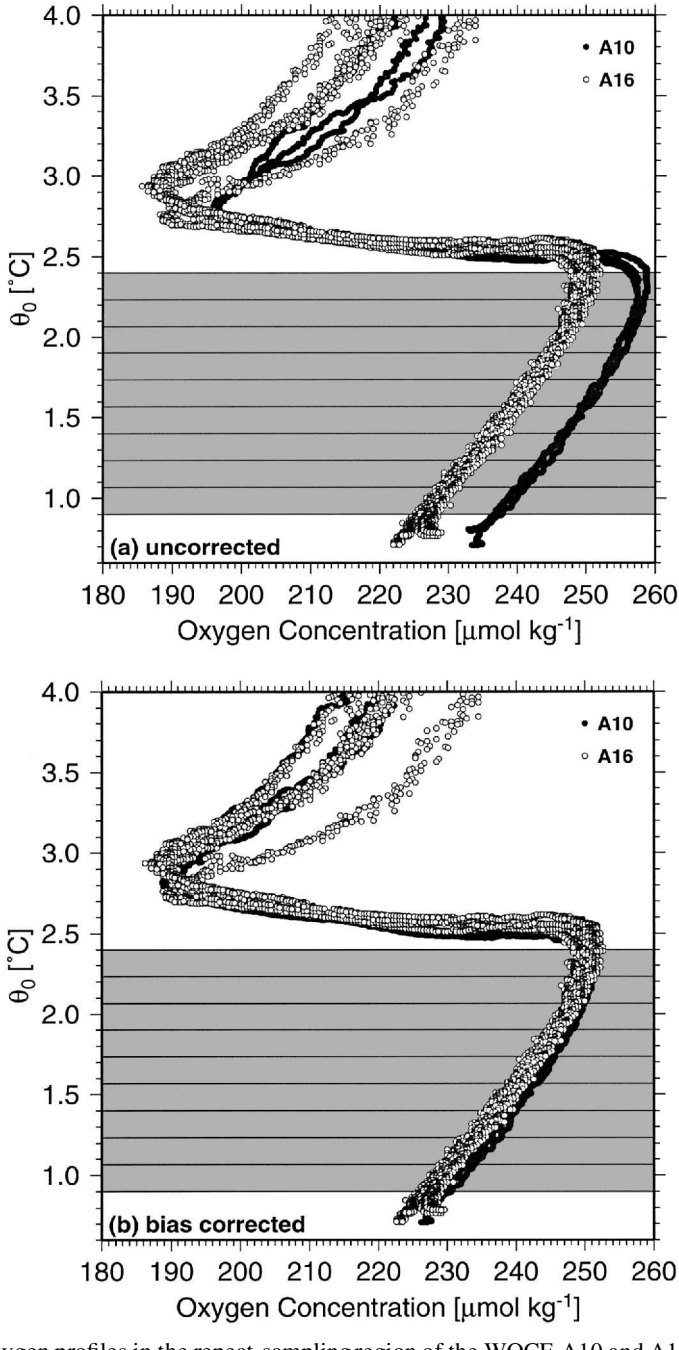

Figure 12. Oxygen profiles in the repeat-sampling region of the WOCE A10 and A16 sections near 30S/25W; gray area shows temperature range of small oxygen scatter; horizontal lines indicate 10 isotherms on which the bias adjustments are carried out. (a) Uncorrected data. (b) Bias-corrected data; (c) Scale-corrected data.

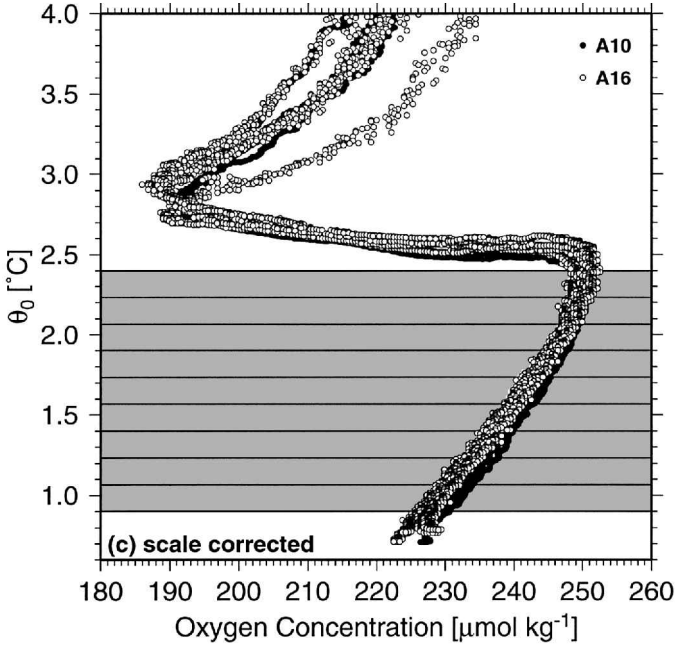

Figure 12. (Continued)

0.1°C fulfilling all these criteria were removed from the data set, leaving 103, 79 and 88 for salinity, oxygen and silicate, respectively. (No valid repeat-sampling region is available for the Romanche 2 oxygen data, which are, therefore, not included in the climatology.)

Each repeat-sampling region contributes an equation to a linear system that is solved by least squares in order to determine (additive) bias and (multiplicative) scale corrections for each section (Johnson *et al.,* 2001). The equations are weighted by the inverse of a measure of the regional tracer scatter, taken here from the larger of the two standard deviations (one per section) of the tracer concentrations on a given isotherm. In repeat-sampling regions with few stations per section the resulting standard deviations can be unrealistically low and a lower limit was selected for each tracer from the mode of histograms of the standard deviations in all repeat-sampling regions (0.0005 for salinity, 0.6 μmol kg^{-1} for oxygen, 0.3 μmol kg^{-1} for silicate). The resulting systems of linear equations are formally overdetermined but, in the case of the additive biases, rank-deficient because of the lack of an absolute standard. This problem is solved by calculating the minimum-norm solution. In contrast to Johnson *et al.* (2001) we estimate the correction uncertainties from 10 separate adjustments carried out on regularly spaced isotherms in the temperature ranges of low variability (horizontal lines in Fig. 12), rather than from the formal solution covariance matrices. (The bottle data are linearly interpolated onto the isotherms while nearest-neighbor subsampling is used for the CTD data.) Additive biases are calculated for salinity, oxygen and silicate. In the case of oxygen and silicate additive bias corrections can result in

Table 3. Bias and scale corrections for the sections listed in Table 2; standard deviations are given in parentheses.

		Oxygen		Silicate	
Data set	Salinity bias [10^{-3}]	Bias [μmol kg^{-1}]	Scale Correction	Bias [μmol kg^{-1}]	Scale Correction
WOCE A07	0.3 (0.2)	1.6 (0.2)	0.992 (0.001)	0.4 (0.1)	0.991 (0.002)
WOCE A08	−2.9 (0.3)	n/a	n/a	−4.0 (0.8)	1.081 (0.006)
WOCE A09	−2.9 (0.2)	−1.4 (0.1)	1.006 (0.001)	−1.0 (0.3)	1.018 (0.004)
WOCE A10	−0.7 (0.4)	7.2 (0.4)	0.970 (0.003)	−1.8 (0.8)	1.034 (0.007)
WOCE A11	−1.0 (0.3)	−4.7 (0.4)	1.022 (0.002)	−2.6 (0.4)	1.025 (0.004)
WOCE A13	0.6 (0.3)	−0.2 (0.2)	1.001 (0.001)	−1.5 (0.2)	1.024 (0.003)
WOCE A14	2.2 (0.3)	−1.1 (0.1)	1.005 (0.001)	−1.3 (0.2)	1.028 (0.002)
WOCE A15	−2.6 (0.3)	−1.0 (0.1)	1.004 (0.001)	−0.5 (0.3)	1.005 (0.004)
WOCE AR15	−2.6 (0.3)	−1.0 (0.1)	1.004 (0.001)	−0.5 (0.3)	1.005 (0.004)
WOCE A16	−1.7 (0.3)	−0.6 (0.5)	1.002 (0.003)	2.2 (0.9)	0.972 (0.004)
WOCE A17	0.8 (0.3)	−0.6 (0.5)	1.003 (0.002)	1.2 (0.8)	0.984 (0.009)
WOCE A23	1.5 (0.6)	−5.3 (0.6)	1.025 (0.001)	2.0 (0.7)	0.944 (0.014)
AJAX 1	1.6 (0.6)	2.4 (0.3)	0.989 (0.001)	0.6 (0.2)	0.989 (0.002)
BEST 2	0.1 (1.2)	1.0 (0.4)	0.995 (0.002)	n/a	n/a
Discovery 1987	1.9 (0.7)	n/a	n/a	n/a	n/a
Oceanus 133 (11S)	2.9 (0.3)	−0.7 (0.6)	1.002 (0.002)	1.3 (0.3)	0.975 (0.002)
Oceanus 133 (24S)	4.3 (0.6)	1.4 (0.5)	0.993 (0.002)	0.4 (0.4)	0.994 (0.004)
Oceanus 133 (30W)	4.3 (0.6)	1.4 (0.5)	0.993 (0.002)	0.4 (0.4)	0.994 (0.004)
SAVE 1	−0.9 (0.4)	0.1 (0.4)	1.000 (0.002)	1.0 (1.1)	0.989 (0.011)
SAVE 2	−0.2 (0.1)	−0.6 (0.1)	1.003 (0.001)	0.3 (0.3)	0.992 (0.004)
SAVE 3	−1.0 (0.1)	1.2 (0.5)	0.993 (0.004)	0.0 (0.3)	0.999 (0.006)
SAVE 4	−2.9 (0.4)	−0.1 (0.3)	0.999 (0.001)	1.4 (0.2)	0.981 (0.002)
SAVE 5	−0.3 (0.3)	0.1 (0.2)	0.999 (0.002)	2.8 (0.7)	0.964 (0.006)
James Clark Ross 65	−1.0 (0.2)	n/a	n/a	n/a	n/a
Meteor 41/3	−0.8 (0.4)	n/a	n/a	n/a	n/a
Romanche 2	3.1 (0.8)	n/a	n/a	n/a	n/a

negative values in regions of low tracer concentrations (e.g. Johnson *et al.,* 2001); therefore, we also calculate scale corrections for these tracers, using the same weighing of the linear systems as for the bias corrections. (In this study only the additive biases are used; the corresponding maps constructed from scale-corrected tracer fields are visually nearly indistinguishable; c.f. Fig. 12b, c.) Table 3 lists the resulting measurement biases and scale corrections, and a fully corrected oxygen map at 2500 m is shown in Figure 11b.

b. Spatial filtering and interpolation

In order to reduce the file sizes and increase processing speed the data available at CTD resolution (salinity, oxygen in some sections) are pre-averaged in 50 dbar vertical bins. In order to calculate the gridded fields the data are then linearly interpolated onto the target

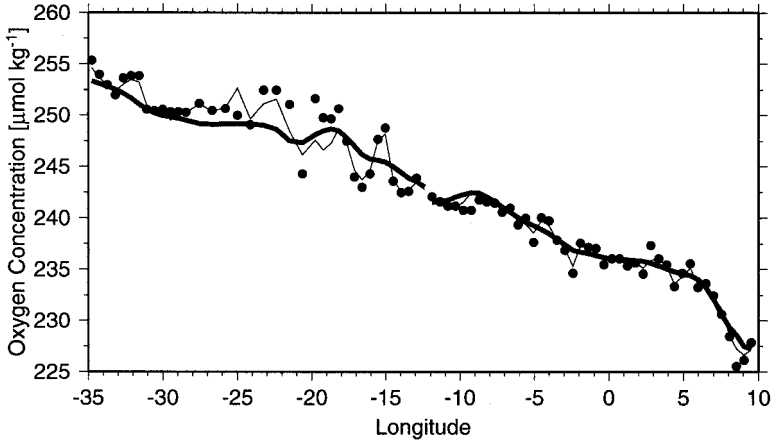

Figure 13. Bias-corrected oxygen concentration at 2500 m along 19S in the WOCE A09 section (bullets) and in the climatology, with and without applying a 1°-Gaussian filter (thick and thin lines, respectively).

isopleths. (In this study isobaths are used throughout; a set of maps on neutral-density surfaces are available at http://www.ocean.fsu.edu/SAC.) In order to simplify the handling of (near-)repeat stations the bias-corrected tracer data are pre-averaged in grids of 0.5° × 0.5° resolution before horizontal interpolation. Grid cells without data are filled by constructing harmonic surfaces (which allow extrema only at control-data points). Regions where the target isosurface intersects the bathymetry of Smith and Sandwell (1997) (version 8.2 averaged onto the same 0.5° × 0.5° grid) are shaded solid without contours in all maps. Independent harmonic surfaces are constructed for the Brazil, Argentine, Cape, and Angola basins before contouring. The continuity of tracer contours across the Mid-Atlantic Ridge crest (e.g. Fig. 1) is, therefore, an indication of the internal consistency of the deep tracer fields.

The cuspiness of some of the contours apparent in Figure 11b (e.g. near 19S between 15 and 30W) is an aliasing effect due to the discretization of the oxygen data onto a small number of contour levels. The discretized data do not retain information about fluctuations within a contour level and over-emphasize fluctuations across contour levels. This effect occurs primarily in regions where the tracer gradients are small. Figure 13 shows a scatter plot of the 19S oxygen concentrations in the WOCE A09 section at 2500 m (bullets), as well as the corresponding values in the 0.5° × 0.5°-resolution climatology (thin line). Because we are primarily concerned with the large-scale tracer distributions, which are characterized by patterns with scales of several hundreds of km, the station-to-station fluctuations are considered noise. For the tracer maps shown in Section 2 the 0.5° × 0.5°-pre-averaged data were therefore smoothed using a Gaussian filter of width $\sigma = 1°$ before the harmonic surfaces were constructed (heavy line in Fig. 13). In general, the mapped data closely follow the measurements of individual sections and there are no

apparent artifacts at section crossovers. The spatially filtered tracer maps therefore objectively represent the large-scale tracer distributions while approaching the smoothness typical of manually contoured tracer maps.

REFERENCES

Armi, L. and H. Stommel. 1983. Four views of a portion of the North Atlantic subtropical gyre. J. Phys. Oceanogr., *13,* 828–857.

DeMadron, X. D. and G. Weatherly. 1994. Circulation, transport and bottom boundary layers of the deep currents in the Brazil Basin. J. Mar. Res., *52,* 583–638.

Ganachaud, A. 1999. Large scale oceanic circulation and fluxes of freshwater, heat, nutrients and oxygen, Ph. D. thesis, MIT/WHOI Joint Program.

Gill, A. E. 1982. Atmosphere-Ocean Dynamics, Academic Press, San Diego, CA, 662 pp.

Gordon, A. L. and K. T. Bosley. 1991. Cyclonic gyre in the tropical South Atlantic. Deep-Sea Res. A, *38,* S323–S343.

Gouretski, V. V. and K. Jancke. 2001. Systematic errors as the cause for an apparent deep water property variability: Global analysis of the WOCE and historical hydrographic data. Prog. Oceanogr., *48,* 337–402.

Hogg, N. G. and W. B. Owens. 1999. Direct measurement of the deep circulation within the Brazil Basin. Deep-Sea Res. II, *46,* 335–353.

Johnson, G. C., P. E. Robbins and G. E. Hufford. 2001. Systematic adjustments of hydrographic sections for internal consistency. J. Atmos. Ocean Tech., *18,* 1234–1244.

Müller, T. J. and G. Siedler. 1992. Multi-year current time-series in the eastern North Atlantic Ocean. J. Mar. Res., *50,* 63–98.

Polzin, K. L., J. M. Toole, J. R. Ledwell and R. W. Schmitt. 1997. Spatial variability of turbulent mixing in the abyssal ocean. Science, *276,* 93–96.

Reid, J. L. 1989. On the total geostrophic circulation of the South Atlantic Ocean: flow patterns, tracers and transports. Prog. Oceanogr., *23,* 149–244.

Richardson, P. L. and S. L. Garzoli. 2003. Characteristics of intermediate water flow in the Benguela current as measured with RAFOS floats. Deep-Sea Res. II, *50,* 87–118.

Roemmich, D. and P. Sutton. 1998. The mean and variability of ocean circulation past northern New Zealand: Determining the representativeness of hydrographic climatologies. J. Geophys. Res., *103,* 13041–13054.

Roemmich, D. and C. Wunsch. 1985. Two transatlantic sections—meridional circulation and heat-flux in the subtropical North Atlantic Ocean. Deep-Sea Res., *32,* 619–664.

Sherman, J., R. E. Davis, W. B. Owens and J. Valdes. 2001. The autonomous underwater glider "Spray." IEEE J. Ocean. Eng., *26,* 437–446.

Smith, W. H. F. and D. T. Sandwell. 1997. Global seafloor topography from satellite altimetry and ship depth soundings. Science, *277,* 1956–1962.

Speer, K. G., G. Siedler and L. Talley. 1995. The Namib Col Current. Deep-Sea Res. I, *42,* 1933–1950.

Suga, T. and L. D. Talley. 1995. Antarctic Intermediate Water circulation in the tropical and subtropical South Atlantic. J. Geophys. Res., *100,* 13441–13453.

Talley, L. D. and G. C. Johnson. 1994. Deep, zonal subequatorial currents. Science, *263,* 1125–1128.

Talley, L. D., D. Stammer, and I. Fukumori. 2001. Towards a WOCE synthesis, *in* Ocean Circulation and Climate, G. Siedler, J. Church and J. Gould, eds., Academic Press, 525–545.

Treguier, A.-M., N. G. Hogg, M. Maltrud, K. Speer and V. Thierry. 2003. The origin of deep zonal flows in the Brazil Basin. J. Phys. Oceanogr., *33,* 580–599.

Tsuchiya, M., L. D. Talley and M. S. McCartney. 1994. Water-mass distributions in the western

South-Atlantic—A section from South Georgia Island (54S) northward across the equator. J. Mar. Res., *52,* 55–81.

Vanicek, M. and G. Siedler. 2002. Zonal fluxes in the deep water layers of the western South Atlantic Ocean. J. Phys. Oceanogr., *32,* 2205–2235.

Warren, B. A. and K. G. Speer. 1991. Deep circulation in the eastern South Atlantic Ocean. Deep Sea Res., *38,* 281–322.

Weatherly, G., M. Arhan, H. Mercier and W. Smethie, Jr. 2002. Evidence of abyssal eddies in the Brazil Basin. J. Geophys. Res., *107,* 10.1029/2000JC000648.

Wunsch, C. 1981. Low-frequency variability of the sea, *in* Evolution of Physical Oceanography, B. A. Warren and C. Wunsch, eds., M.I.T. Press, 342–374.

—— 1996. The Ocean Circulation Inverse Problem, Cambridge University Press, 442 pp.

—— 1997. The vertical partition of oceanic horizontal kinetic energy. J. Phys. Oceanogr., *27,* 1770–1794.

—— 2001. Global problems and global observations, *in* Ocean Circulation and Climate, G. Siedler, J. Church and J. Gould, eds., Academic Press, 47–58.

Wüst, G. 1935. Schichtung und Zirkulation des Atlantischen Ozeans. Die Stratosphäre., Wissenschaftliche Ergebnisse der Deutschen Atlantischen Expedition auf dem Forschungsund Vermessungsschiff "Meteor" 1925–1927, *6,* 180 pp. Reprinted as The Stratosphere of the Atlantic Ocean, W. J. Emery, ed., 1978, Amerind, New Delhi, 112 pp.

Zhang, H. M., and N. G. Hogg. 1992. Circulation and water mass balance in the Brazil Basin. J. Mar. Res., *50,* 385–420.

Received: *19 August, 2003;* revised: *23 December, 2003.*